Direct links between hygroscopicity and mixing state of ambient aerosols: Estimating particle hygroscopicity from their single particle mass spectra

Xinning Wang[1], Xiaofei Wang*[1,2] and Xin Yang*[1,2]

[1] Shanghai Key Laboratory of Atmospheric Particle Pollution and Prevention, Department of Environmental Science and Engineering, Fudan University, Shanghai 200433, China

[2] Shanghai Institute of Pollution Control and Ecological Security, Shanghai 200092, China

*To whom correspondence should be addressed.
Correspondence to:
Xiaofei Wang
Email: xiaofeiwang@fudan.edu.cn Tel: +86-21-31242526
Xin Yang
Email: yangxin@fudan.edu.cn Tel: +86-21-31245272

23 ***ABSTRACT***

24 Hygroscopicity plays a crucial role in determining aerosol optical properties and aging

25 processes in the atmosphere. We investigated submicron aerosol hygroscopicity and

26 composition by connecting an aerosol time-of-flight mass spectrometer (ATOFMS) to the

27 downstream of a hygroscopic tandem differential mobility analyzer (HTDMA), to

28 simultaneously characterize hygroscopicities and chemical compositions of ambient aerosols

29 in Shanghai, China. Major particle types, including biomass burning, EC, Dust/Ash, organics

30 particles, cooking particles and sea salt, were shown to have distinct hygroscopicity

31 distributions. It is also found that particles with stronger hygroscopicities were more likely to

32 have higher effective densities. Based on the measured hygroscopicity-composition relations,

33 we developed a statistical method to estimate ambient particle hygroscopicity just from their

34 mass spectra. This method was applied to another ambient ATOFMS dataset sampled from

35 September 12nd to 28th, 2012 in Shanghai, and it is found that ambient particles were present in

36 three major hygroscopicity modes, whose growth factors at relative humidity 85% peaked at

37 1.05, 1.42 and 1.60, respectively. The temporal variations of the estimated particle

38 hygroscopicity were consistent with the back-trajectory analysis and atmospheric visibility

39 observations. These hygroscopicity estimation results with single particle mass spectra analysis

40 can provide critical information on particulate water content, particle source apportionment and

41 aging processes.

42

1. INTRODUCTION

43

44 Atmospheric particles have critical influences on climate and the environment. They affect

45 climate by directly interacting with sunlight and changing the energy balance of earth's

46 atmosphere (Facchini et al., 1999;Lohmann and Feichter, 2005). Additionally, they act as cloud

47 condensation nuclei or ice nuclei and impact cloud formation (Lohmann et al., 2007). Aerosol

48 particles also participate many important atmospheric reactions (Gard et al., 1998;Qiu and

49 Zhang, 2013). The climate-relevant properties and chemical reactivity of aerosols are largely

50 determined by their hygroscopic property. In the ambient condition the hygroscopic growth of

51 particles introduce aqueous surface to particles and their optical effects are importantly altered

52 (Cheng et al., 2008;Titos et al., 2014), which exerts impacts on atmospheric aging processes of

53 particles and visibility degradation (Qu et al., 2015;Liu et al., 2012;Qiu and Zhang, 2013;Wang

54 et al., 2009;Chen et al., 2012;Li et al., 2018).

55 Atmospheric particles are a mixture of a complicated variety of chemical compounds. The bulk

56 chemical composition of particulate matter (PM) usually refers to its dry composition (Li et al.,

57 2016;Herich et al., 2011). However, in ambient condition the particulate water is also an

58 important constitution of PM which has not been accounted for in conventional gravitational

59 analysis. The mass of particulate water may be times higher than the total mass of dried PM at

60 elevated RHs (Swietlicki et al., 2008). The factors that affect water contents in particles include

61 the particle hygroscopicity, the particle size distributions and ambient RH. Particle

62 hygroscopicity determines the particle's ability to hygroscopic growth. It direclty relates to

63 particle composition and size. To accurately predict particulate water content, a detailed

64 knowledge on both of particle hygroscopicity and composition is needed (Gysel et al.,

65   2007;Sjogren et al., 2008;Laborde et al., 2013;Healy et al., 2014).

66   Aerosol hygroscopicity could be determined quantitatively by techniques such as the

67   Hygroscopic Tandem Differential Mobility Analyzer (HTDMA) (Swietlicki et al., 2008).

68   Previous studies have obtained particle hygroscopicity and chemical composition in the same

69   time by deploying HTDMA and chemical composition measurements in parallel (Gysel et al.,

70   2007;Sjogren et al., 2008;Laborde et al., 2013). The measured hygroscopicity was compared

71   with the reconstructed values using the mixing rules of variant compositions (Gysel et al., 2007).

72   The hygroscopicity reconstructed in this way is representing the averaged hygroscopicity of

73   ensembled particles and therefore could not reflect the mixing states of particles (Healy et al.,

74   2014). Ambient studies suggested that atmospheric aerosols were commonly externally mixed,

75   as shown by the separated modes in hygroscopicity distributions (Swietlicki et al.,

76   2008;Massling et al., 2007;Liu et al., 2011). The alternative way to obtain simultaneous

77   information on hygroscopicity and composition is connecting the HTDMA with particle

78   composition measurement techniques in tandem (Buzorius et al., 2002;Zelenyuk et al.,

79   2008;Herich et al., 2008;Laborde et al., 2013). In this configuration, the HTDMA acts as

80   hygroscopicity selector, with hygroscopicity segregated particles being analyzed subsequently

81   by other techniques. More direct connection between hygroscopicity and composition could be

82   established in this way. For particle composition measurement, sensitive methods such as single

83   particle mass spectrometers are preferred since they can analyze particles in low concentrations

84   in the outflow of HTDMA (Herich et al., 2008;Herich et al., 2009). The merit of single particle

85   techniques is that particle mixing state is preserved during analysis (Healy et al., 2014).

86   Only a few previous studies have reported simultaneous characterization of hygroscopicity and

87 composition using the tandem method (Herich et al., 2008;Herich et al., 2009;Buzorius et al.,

88 2002;Zelenyuk et al., 2008). Zelenyuk et al.(Zelenyuk et al., 2008) connected HTDMA and a

89 single particle mass spectrometer SPLAT in series to perform multiple measurement of aerosol

90 composition, hygroscopicity and effective density. Herich et al. have firstly applied the

91 HTDMA-ATOFMS system to investigate particle composition as a function of hygroscopicity

92 in Switzerland (Herich et al., 2008) and then in a subarctic site (Herich et al., 2009). In a

93 preliminary study, we applied HTDMA-ATOFMS to characterize chemical compositions of

94 ambient particles with a few hygroscopicities (Wang et al., 2014). However, this obtained

95 dataset is not sufficiently large to provide a hygroscopicity distribution for each aerosol particle

96 type. Therefore, the primary objective of the present study is to establish thorough connections

97 between hygroscopicity and single particle signatures, which could be utilized to predict

98 hygroscopicity of ambient particles. Here we conducted a comprehensive HTMDA-ATOFMS

99 characterization experiment with a more complete GF range (GF 0.9~1.7, 85% RH), which

100 accounts for a main number fraction of atmospheric particles in urban atmosphere (Liu et al.,

101 2014;Liu et al., 2011;Ye et al., 2013) . Moreover, we developed and tested a method that utilize

102 the established dataset to estimate the hygroscopicity of ambient particles analyzed by

103 ATOFMS.

104 ***2. EXPERIMENTAL SECTION***

105 **2.1. HTDMA**

106 The custom-built HTDMA (Ye et al., 2009;Angelino et al., 2001) consists of two DMAs and a

107 humidifier (Figure 1). Aerosol was dried before entering HTDMA (RH ~10%) by a diffusional

108 silica gel tube. The dried aerosol reached its charge equilibrium in a Kr-85 neutralizer. The

109 DMA1 (Model 3081, TSI Inc.) selected particles based on their electrical mobility size D_{dry}.

110 Then, the monodisperse particles grew in a Nafion humidifier (RH=85%). The sizes of

111 humidified particles D_{RH} was scanned by the second DMA and a CPC. The sheath flow rate in

112 DMA2 (3 l/min) was regulated by mass flow controller. The RH of the DMA2 sheath flow was

113 managed to match the humidifier (85% RH) by adjusting the water-saturated air. The DMAs,

114 the humidifier and other parts were installed in thermostatic chamber in which temperature was

115 controlled to 25℃. The total aerosol flow was 0.4 L/min (the sum flow rate of the CPC, 0.3

116 L/min and the ATOFMS, 0.1 L/min). Aerosol residence time in humidifier was ~10 s. PSL

117 spheres of known size and $(NH_4)_2SO_4$ salt were used to calibrate the HTDMA.

118 **2.2. ATOFMS**

119 The principle functional parts of ATOFMS (Model 3800, TSI. Inc) is illustrated in Figure 1.

120 After particles entered the inlet orifice of ATOFMS, they were focused into narrow beam

121 through successive expansions and contractions in the aerodynamic focusing Lens (AFL).

122 Particles leaving the AFL have drifting velocities which are depended on their vacuum

123 aerodynamic sizes. In ATOFMS sizing region the particles pass through two orthogonally

124 oriented continuous lasers (Nd:YAG, 532 nm) to scatter light. The scattered light generates two

125 pulses in two photomultiplier tubes (PMT) and the signal delay between the two pulses is used

126 to calculate particle velocity considering the distance between two lasers is known. Particle

127 velocity information was also used to trigger ionization laser (Nd:YAG, 266 nm) at appropriate

128 time to ionize individual particles. The ions are recorded by a dual polar time-of-flight mass

129 spectrometer to generate positive and negative mass spectra for each particle. More details of

130   ATOFMS were described elsewhere (Gard et al., 1997;Su et al., 2004).

2.3. Field sampling

132   During Feb-26 to Mar-7, 2014, the HTDMA-ATOFMS characterization was performed at the

133   building of department of environmental science and technology in Fudan university (31°18'N,

134   121°29'E). Aerosol inlet was installed at the building roof about 6 m above the ground. The

135   Fudan campus was influenced by local emissions sources from transportation, residential,

136   business and cooking activities from surrounding areas which can be viewed as an urban

137   environment. A period of ambient ATOFMS data, which persisted from Sep-12 to Sep-28, 2012,

138   was obtained at the same site in Fudan campus.

139   The sampling procedure was similar to our previous study (Wang et al., 2014). The HTDMA

140   GF distributions obtained during sampling intermittence usually show two hygroscopicity

141   modes. The first mode centered at GF ~1.05 and the second mode at GF ~1.45 at RH 85%,

142   which will be termed as Near-Hydrophobic (NH) and More-Hygroscopic (MH) mode,

143   respectively. These modes were also typically found in other types of environment (Liu et al.,

144   2011;Swietlicki et al., 2008). The majority of particles (>97 %) were shown to have growth

145   factors in 0.9-1.7 range. Therefore, in this study we preselected particles with GFs from 0.9 to

146   1.7 (0.1 GF step) in HTDMA for ATOFMS characterizations.

147   To set the desired GFs, the two DMAs in HTDMA system were maintained at fixed diameters

148   D_{dry}, D_{RH} according to GF=D_{RH}/D_{dry}. The DMAs were kept to select the desired diameters

149   before significant number of particle were chemical analyzed by ATOFMS. In this study the

150   DMA1 (D_{dry}) was set to 250 nm, while the DMA2 (D_{RH}) was set to diameters as shown in Table

151 1, where the length of sampling duration, the number analyzed particles are given. The number

152 of particles analyzed by ATOFMS was affected by the ambient particle number concentrations.

153 Because the particle concentrations in the outflow of HTDMA are generally low and even lower

154 at some GFs, longer sampling time was planned to obtain statistically significant particle

155 numbers (See the CPC concentrations in Figure S1). Usually the ATOFMS has lower detection

156 efficiencies at smaller than 250 nm range due to the reduced scattering efficiency, while larger

157 particles usually have less number concentrations. Therefore, the selection of D_{dry} as 250nm is

158 a compromise between the two issues (Wang et al., 2014;Herich et al., 2008;Herich et al., 2009).

159

160 **Table 1. Statistics of the D_{RH}, GF, sampling duration and the number of chemically analyzed**

161 **particles by ATOFMS (D_{dry} = 250 nm, RH = 85%).**

D_{RH} (nm)	225	250	275	300	325	350	375	400	425
Growth Factor	0.9	1.0	1.1	1.2	1.3	1.4	1.5	1.6	1.7
Duration (hours)	42	67	11	20	8	11	34	20	11
Number of spectra detected	742	1665	709	1401	2330	4469	6399	723	262

162

163 **2.4. Estimation of ambient particle hygroscopicity**

164 When inspecting particle mass spectra obtained from HTDMA-ATOFMS experiment, it is

165 recognized that most of produced spectra were also frequently present in ATOFMS ambient

166   characterizations. This fact forms the basis of the idea to assign similar GF to ambient particles

167   if they have similar composition as in HTDMA-ATOFMS experiment.

168   To estimate hygroscopicity of ambient single particles, we compare the ambient particle mass

169   spectra with those obtained in HTDMA-ATOFMS experiment similarly as in ART-2a algorithm

170   (Song et al., 1999). In ATOFMS particle spectra, some metal (such as Na, K, Fe) were

171   producing inappropriately large peaks due to higher ionization efficiencies. This problem was

172   relieved by taking the 0.5 power (square root) of peaks intensities. After this treatment the

173   relative intensities of largest peaks were suppressed the while smaller peaks (such as organic

174   peaks) increased relatively in the evaluation of spectra similarities. Then we searched the

175   candidate particles in HTDMA-ATOFMS data which produced the highest similarities with the

176   atmospheric particle (similarities in the range of 95% to 100% maximum similarity). Since each

177   item of mass spectra acquired by HTDMA-ATOFMS was associated with a GF, we obtained a

178   collection of discrete GF values (from 0.9 to1.7 spaced by 0.1) that were the most probable

179   candidate GFs. The estimated GF of the atmospheric particle was determined to be the weighted

180   mean of the candidate GFs, with weights being the number percentages of candidate particles

181   happened in each discrete GF groups:

182
$$GF_{pred} = \frac{\sum GF_i \cdot F_i}{\sum F_i}$$

183   where: GF_{pred}= the estimated GF of atmospheric particle, GF_i= GF value from 0.1 to 1.7

184   interspaced by 0.1, F_i= number percentages of the candidate particles in each GF group.

185   From the descriptions above, this method is a statistical approach to find the most probable

186   hydroscopicity for each single particle, rather than estimating chemical compositions in

187 individual particles and then predicting particle hygroscopicity using the assumed composition,

188 as previously applied by (Healy et al., 2014). The latter approach is based on Zdanovskii-

189 Stokes-Robinson mixing roles, and it needs to assume a chemical composition for each single

190 aerosol particle, which might not be reliable due to the qualitative nature of ATOFMS analysis.

191 However, the new approach developed in this study infer particle hygroscopicity by comparing

192 the mass spectra of ambient particles with particles whose hygroscopicity has already been

193 experimentally determined by HTDMA. Therefore, this method derives GF from measured GF

194 values and the possible artifacts caused by assumptions are obviated.

3. RESULTS AND DISCUSSIONS

195

3.1. Hygroscopicity distribution of particle types

196

197 The sampled aerosols with similar mass spectra are grouped together to form many particle

198 types. The majority of analyzed particles were eventually grouped into 9 types, namely Biomass,

199 Fresh EC, Aged EC, Dust/Ash, HMOC, Amine-rich, Ammonium/OC, Cooking and Sea salt

200 types. Figure 2 presents the average mass spectra, particle numbers detected at different GF

201 stages for each types. Since the numbers of analyzed particle in each GF bin are not a constant

202 (Table 1), the normalized particle numbers by the total particle numbers in each GF bin were

203 calculated to show their occurrence probability (Fig. 2).

3.1.1. Particle types and GF distributions

204

205 As illustrated in Fig. 2, Biomass type particles have characteristic peaks at -26(CN), -42(CNO),

206 -59($C_2H_3O_2$), -73($C_3H_5O_2$) in negative spectra and dominant potassium peak at 39K and clusters

207 at 113(K_2Cl) or 213(K_3SO_4) (Silva et al., 1999). During this study, the HTDMA-ATOFMS

208   system detected 547 biomass particles which account for 2.9% of total analyzed particles.

209   Despite the small number, the hygroscopicity of biomass particles is low in that the majority of

210   biomass particles (87%) were detected in GF <1.2 range. On average the biomass particle type

211   contribute 2.9% of analyzed particle numbers in this GF range, with peak number fraction

212   occurred at GF 1.1 (19%), as shown in Figure 2 (a). Similar hygroscopicity pattern of biomass

213   particles is reported previously (Rissler et al., 2006;Martin et al., 2013).

214   EC type particles are characterized by a series of elemental carbon peaks at C_n (n=1, 2, 3 …) in

215   the negative and positive spectra. EC is a dominant particle type which accounts for 37.5%

216   (7020 particles) of the analyzed particle number in this study. EC particles distributed broadly

217   from NH to MH range. However, the particle compositions are different in NH and MH

218   hygroscopicity range, where fresh and aged EC dominate, respectively (Figure 2 b-c). Fresh

219   EC particles have not experienced significant aging, with weak or no secondary peaks ($-62NO_3^-$,

220    $-97HSO_4^-$, $18NH_4^+$) in their spectra. Therefore, most of them were in hydrophobic mode

221   (Weingartner et al., 1997). The mass spectra of aged EC showed the internal mixing of

222   secondary matters (nitrate, sulfate, ammonium), which is consistent with their hygroscopic

223   property. The peak intensity variations ($-62NO_3^-$, $-97HSO_4^-$, $18NH_4^+$ and other relevant peaks)

224   in EC spectra were a function of GF. A gradual increase of secondary peak intensities in GF 0.9

225   - 1.2 range was observed (Figure S2).

226   Dust/ash type particles have inorganic peaks of salts and metals oxides (Wang et al.,

227   2019;Zhang et al., 2009;Dall'Osto et al., 2008). About 7.4% of analyzed particles were

228   classified into this type. Most of dust/ash particles (>85%) were detected in hygroscopic range

229   (GF > 1.3). However, Dust/ash particles with Al-Si signals were clearly enriched in NH mode

230   (Wang et al., 2014), with the highest detection probability at GF 1.1, as shown in Figure S3.

231   The Al-Si particles are assumed to be soil dusts according to their reported low hygroscopicity

232   (Koehler et al., 2009).

233   The spectra of HMOC type particles contain organic peaks in higher m/z range (>150). This

234   type accounts for 2.6% of total number of analyzed particles. Within the HMOC type, 10%

235   particles have identifiable polycyclic aromatic hydrocarbons (PAH) peaks in their positive

236   spectra and 7% produce high mass signals in negative spectra (Denkenberger et al., 2007). Most

237   of HMOC particles (95%) showed low hygroscopicity (GF<1.2), with peak number fractions

238   of 15% at GF 1.0.

239   Amine-rich type particles produce amine peaks at +59(C_3H_9N), +86($C_5H_{12}N$) and +101($C_6H_{15}N$)

240   (Angelino et al., 2001;Pratt et al., 2009). About 20% of analyzed particles are classified in this

241   type. As found previously (Wang et al., 2014), Amine-rich particles are generally very

242   hydrophilic with the highest detection probability occurred within GF >1.5 range. Short alkyl

243   chain aliphatic amines are basic and have relatively high vapor pressures, therefore their

244   presence in particles most likely occur in the form of aminium salts, whose formation is greatly

245   favored in the presence of particulate water (Angelino et al., 2001;Chen et al., 2019). It is found

246   that 77% Amine-rich particles were internally mixed with sulfate or nitrate.

247   Ammonium/OC type particles demonstrate some similarities to biomass particles, since a

248   strong, dominant potassium peak ^{39}K exist in positive spectra and organic peaks present in

249   lower mass range (45-80). However, this type of particles also produced much more intense

250   ammonium peak at $^{18}NH_4^+$ and significant sulfate peak ($^{-97}HSO_4$). In addition, the ^{-26}CN or $^-$

251   ^{42}CNO peaks, which are present in biomass particles, were absent or very weak, suggesting that

252   biomass burning is not their source. The hygroscopicity pattern of ammonium/OC particles was

253   quite unique. As shown in Fig. 2 (g), ammonium/OC particles are contributing significantly to

254   moderate hygroscopicity range (GF 1.1-1.3), with maximum number contribution of 25% at

255   GF 1.2, a GF at the trough between NH and MH mode. Based on their mass spectral signature

256   and the published ATOFMS characterizations, it is possible that the ammonium/OC particles

257   might be from coal burning sources (Healy et al., 2010). The organics in ammonium/OC

258   particles could be probably produced from inefficient combustion of coal (Wang et al., 2013).

259   The strong ammonium peak in this particle type may be generated in SCR denitration process

260   since the ammonia is usually added in such process. These particles were not likely to be deeply

261   aged particles, because their hygroscopicity was only moderate.

262   Cooking is a significant source of primary organic aerosol (POA) in urban regions (Crippa et

263   al., 2013;Robinson et al., 2006). Zhang et al. estimated that up to 35% of POA are attributed to

264   cooking aerosol during meal hours (Zhang et al., 2007). Cooking particles around the site was

265   likely to be significant considering that the Fudan campus is located in a heavily populated area.

266   The ATOFMS characterization of cooking particles have been performed previously (Silva,

267   2000;Dall'Osto et al., 2013). The markers at -255($C_{16}H_{32}O_2$, palmitic), -281 ($C_{17}H_{34}O_{2,}$ oleic

268   acid) in the negative spectra were used to identify Cooking type of particles (Dall'Osto and

269   Harrison, 2012;Silva, 2000). We identified 861 (%4.6 of total) cooking particles. As shown in

270   Figure 2(h), this particle type had extreme low hygroscopicity and 99% of them were detected

271   in GF<1.1 range. Based on the ATOFMS particle number, cooking particles contribute 19%

272   particle concentrations of NH mode, with its peak contribution occurred at GF 0.9 (49%). It is

273   noted that GF 0.9 does not necessarily indicate a particle shrinkage in diameter. Cooking

274   particles might become more spherical in elevated RH, resulting in smaller mobility diameters.

275   This phenomenon was also observed for other organic particles (Shi et al., 2012). The low

276   hygroscopicity of cooking particles is consistent with their organic composition indicated by

277   the fatty acids (-171, -255, -279,-281) and HOA (+55, +57) peaks in the spectra. The detection

278   of cooking particles in NH mode is a complement to the assumption that combustion sources

279   are the major source of NH particles (Swietlicki et al., 2008;Laborde et al., 2013;Herich et al.,

280   2009).

281   Sea salt particle type is an important type of particles in ambient air in coastal areas(Herich et

282   al., 2009;Gard et al., 1998). Their mass spectra contain a major peak at ^{23}Na and other peaks

283   at $^{62}Na_2O$, $^{63}Na_2OH$, $^{81}Na_2Cl$. The hygroscopicity of sea salt is of interest since it is critical

284   in the aerosol-cloud interactions in marine and coastal areas (Andreae and Rosenfeld,

285   2008;Massling et al., 2007). Although only 314 sea salt particles (1.7 %) were detected in this

286   study, their hygroscopicity pattern is rather clear that they were mostly present in the largest

287   GF range (>1.5). The large hygroscopicity of sea salt is also indicated by increased number

288   fractions from 2.6% at GF 1.5 to 19% at GF 1.7, as show in Figure 2 (i). The obtained result

289   here is consistent with HTDMA characterizations in marine environment (Swietlicki et al.,

290   2008;Massling et al., 2007), where sea salt particles made up a clear hygroscopicity mode of

291   the largest GF. The hygroscopicity of sea salt in this study is somewhat different compared with

292   the previous characterization in a subarctic region, where sea salt particles were mainly detected

293   in GF 1.3-1.5 range at 82% RH using HTMDA-ATOFMS (Herich et al., 2009). Therefore sea

294   salt particle properties are variant with locations and other factors (organics in seawater, marine

295 microbiological conditions, aging) should be considered (Facchini et al., 2008;Randles et al.,

296 2004).

297 The impact of aging on sea salt hygroscopicity was investigated. Spectra analysis was

298 performed by correlating sea salt peak intensities with GF. It is known that NaCl in fresh sea

299 salt could react with nitric acid in the atmosphere, with the $NaNO_3$ formed in particles and HCl

300 released (Gard et al., 1998). This chemical transformation is reflected in corresponding change

301 in the sea salt mass spectra. Fresh sea salt produce stronger peaks of positive peak Na_2Cl^+ and

302 negative peak $NaCl_2^-$ in their spectra. With the atmospheric transformation, NaCl is transformed

303 into $NaNO_3$, $Na_2NO_3^+$ and $Na(NO_3)_2^-$ peaks emerge and grow stronger, while NaCl related

304 peaks Na_2Cl^+ and $NaCl_2^-$ decrease or vanish. The statistics of sea salt peak intensities at different

305 GF are shown in Figure 3. Obviously, sea salt particles with smaller GF tend to produce stronger

306 $NaNO_3$ related peaks and weaker NaCl related peaks. This result is an evidence that aged sea

307 salt have reduced hygroscopicity (Herich et al., 2009). The transformation of NaCl into $NaNO_3$

308 could not generate the observed reduction in GF. Similar result was observed in the subarctic

309 site (Herich et al., 2009). It is likely that organics condensed on Sea salt particles and lowered

310 their hygroscopicity.

311 **3.1.2. Particle effective density and hygroscopicity**

312 Simultaneous information on particle effective density and hygroscopicity is rarely reported

313 (Zelenyuk et al., 2008). Fortunately, the particle effective densities and chemical composition

314 can be measured on by HTDMA-ATOMFS system (Figure 4). Obviously, the particles with

315 lower GF had lower effective densities, while the particles with higher GF had a larger effective

316 density, which was finally approaching to ~ 1.5 g cm^{-3} and had much smaller range of effective

317 density deviation, suggesting that a main fraction of particles with high GF were more likely to

318 be aged aerosols that mainly comprised of a mixture of secondary species, such as ammonium

319 sulfate (density: 1.77 g/cm^3) and ammonium nitrate (density: 1.73 g/cm^3). Condensation of

320 ammonium sulfate/nitrate on existing organic carbon aerosols and black carbon aerosols would

321 increase their density. In addition, the densities of ammonium sulfate and ammonium nitrate

322 are similar. Thus, particles with higher mass fraction of ammonium sulfate/nitrate tend to have

323 more similar density, consistent with Figure 4, which shows that the effective density of

324 particles with higher GF had smaller deviation of effective densities.

325 **3.2. Estimating hygroscopicity of ambient particles**

326 Prediction of ambient particle hygroscopicity requires that the HTDMA-ATOFMS dataset have

327 good particle representation and coverage. As discussed in the preceding section, particle types

328 which are normally present during ambient ATOFMS sampling have been characterized in this

329 HTDMA-ATOFMS experiment. Therefore, the HTDMA-ATOFMS dataset in this study can be

330 used to estimate particle hygroscopicity for the majority of ambient particles detected by

331 ATOFMS. In this section, we illustrate an estimation of particle hygroscopicity from a period

332 of ambient ATOFMS data (Sep-12 to Sep-28, 2012), which was collected at Fudan campus, the

333 same site for the HTDMA-ATOFMS experiment.

334 **3.2.1 Hygroscopicity modes in estimated GF**

335 There were 538,983 particles chemically analyzed by ATOFMS during Sep-12 to Sep-28, 2012.

336 The mass spectra in this period was utilized to predict the GF (85% RH) of each individual

337   particle based on the previously described method. With the estimated hygroscopicity of

338   individual particles, several hygroscopicity modes were observed. Figure 5 shows the temporal

339   variation of particle estimated GF. Apparently, at least three hygroscopicity modes were present,

340   with their respective GF peaked at ~1.05, 1.42, and 1.6. The temporal variation of

341   hygroscopicity suggested that the entire period can be roughly divided into four distinct periods

342   of P1, P2, P3 and P4 (as indicated in Figure 5) which have different GF distribution patterns.

343   During P1, the particle numbers were dominated by GF 1.42 mode, while during P2, the GF1.42

344   mode disappeared and GF 1.05 and GF 1.6 modes appeared. The hygroscopicity patter during

345   P3 is similar to P1, but with more distinct GF 1.05 mode. During P4, all three hygroscopicity

346   modes were present.

347   The three hygroscopicity modes derived from ATOFMS data were compared with the GF

348   distributions that obtained from some HTDMA studies (Ye et al., 2013;Ye et al., 2011;Liu et al.,

349   2011;Swietlicki et al., 2008). Previous HTDMA characterizations of particle hygroscopicity in

350   Shanghai shows a near hydrophobic mode with center GF in 1.05~1.1 range at RH 85% (Ye et

351   al., 2011), which is consistent with our estimated hydrophobic GF mode peaked at 1.05. The

352   more hygroscopic mode measured by HTDMA usually centered at GF at 1.43~1.47, while in

353   the estimated GF data, the maximum number occurred at GF around 1.42. The mass spectra of

354   GF 1.6 mode suggest that they usually have high sodium peaks (Figure S2), which were

355   probably sea salt particles. The sea salt mode were reported to be very hygroscopic, with

356   average GF around 2.0 at 90% RH for freshly generated sea salt particles in marine areas

357   (Swietlicki et al., 2008).

358   Since ATOFMS measured particle aerodynamic diameters simultaneously for each particles,

359   we present particle number as a bivariate function of the estimated GF and particle diameter

360   (aerodynamic diameter measured by ATOFMS) in Figure 6. The three particle modes were also

361   apparent in the GF-d_{va} diagram. We also noticed the gradually increased GF of larger particles,

362   which is very consistent with HTDMA observations (Ye et al., 2011;Ye et al., 2013). Healy et.al.

363   have applied a different method to estimate particle hygroscopicity from single particle data

364   using ZSR mixing rule (Healy et al., 2014). In that study particle aerodynamic diameter d_{va} was

365   transformed to equivalent mobility diameter d_m by assuming a particle density. Despite the

366   differences in method, the estimated GF and their distributions are comparable for NH and MH

367   mode particles. However, the presence of sea salt mode was absent in Healy et al., (Healy et al.,

368   2014).

369   As illustrated in Figure 5, different mixing states were observed during P1-P4 periods. Taking

370   the P4 period as an example, the sea salt mode in this period was persistent during this period,

371   while the concentrations of NH mode particles were intermittent with abrupt changes in

372   temporal trend, consistent with the characteristic of local emissions. The number concentrations

373   of MH mode particles increased during nighttime (Figure 5), which probably related to the

374   mixing layers fluctuations. These facts indicate that the estimated hygroscopicity could help to

375   investigate particles' sources, formation mechanisms, and their possible atmospheric aging

376   pathways (Healy et al., 2014;Li et al., 2018;Laborde et al., 2013;Kamilli et al., 2014;Swietlicki

377   et al., 2008).

378   **3.2.2 Hygroscopicity and visibility**

379   Particles with different hygroscopicity have different liquid water content and optical properties.

380 This fact can be demonstrated by correlating the concentrations of particles having different

381 hygroscopicity with atmospheric visibility (Liu et al., 2012;Qu et al., 2015;Chen et al., 2012).

382 We use the visibility data (https://www.wunderground.com/) logged in the Hongqiao airport

383 (31°12'N, 121°20'E) and Pudong airport (31°9.3'N, 121°49'E) during Sep-12 to Sep-28, 2012

384 (see the map in Figure S5). The contemporary visibility data of the two airports correlated

385 strongly (Figure S5), despite the 45 kilometers distance between the two airports. Fudan

386 campus locates roughly between the two airports, so that the average visibility between the two

387 airports was used to represent the visibility at Fudan site. We discriminated the particles into

388 less and more hygroscopic groups at splitting GF of 1.2, with their number concentrations

389 calculated with the same resolution of visibility data, as shown in the upper panel in Figure 5.

390 Except for P2 and P4 periods, when visibility were typically above 10km, an anti-correlation

391 was observed between visibility and particle numbers of more hygroscopic group than less

392 hygroscopic group. The fact could be further demonstrated by splitting particles into finer bins

393 of GF 0.9-1.1, 1.1-1.3, 1.3-1.55, whose number concentrations correlated with visibility (Figure

394 7). For particles in GF 0.9-1.1, there were actually no correlation between their concentrations

395 and visibility (R^2=0.08). For moderate hygroscopic particles (GF 1.1-1.3), the correlation

396 became stronger (R^2=0.34). MH mode particles (GF 1.3-1.55) were found to best anti-correlated

397 with visibility with R^2 =0.58. Thus, these results clearly demonstrated that aerosol particles with

398 higher hygroscopicity could play more important role in affecting visibility.

399 **3.2.3 Sea salt type particles**

400 Sea salt type particles show a unique mode in the GF-d_{va} diagram (Figure 6). We further

401 investigated the relation between characteristics of sea salt particles and the back trajectories of

402 airmass (Figure 8) during period P1-P4 using HYSPLIT mode (Draxler, R. R. and Rolph, G.

403 D.,2003). During period P1, the airmass were relatively stable, and the airmass movement were

404 relatively slow. The local circulation of airmass brought regional aerosol pollution to the

405 sampling site, which was consistent with the elevated concentrations of more hygroscopic (MH)

406 mode particles (Figure 5). During P2, the history of airmass exclusively passed over yellow sea

407 without continental influence. The MH mode particles disappeared and only NH and GF 1.6

408 mode were detected in the predicated GF. Similar as P1, the back trajectories during P3 mainly

409 stayed over continental regions in the mainland of China, resulting regional aerosol pollutions

410 in MH particles to the site and GF 1.6 mode were barely present. During P4, the airmass mainly

411 originated from northeastern part of East China Sea and GF 1.6 mode emerge again.

412 Consequently, the back trajectories support the attribution of GF 1.6 mode to sea salt particles.

413 Figure 9 shows the differential mass spectra between sea salt particles during P1&P3 and during

414 P2&P4, indicating that the sea salt particles, detected in P2 and P4, were relatively fresh, while

415 sea salt particles detected in P1 & P3 period were more aged. Clearly, sea salt particles in P1 &

416 P3 show stronger peaks of $Na(NO_3)_2^-$, $Na_2NO_3^+$, NO_3^-, while sea salt particles in P2 & P4 show

417 stronger NaCl related peaks (Figure 9). This result indicates that sea salt in P1&P3 experienced

418 more aging in the atmosphere. The right panel in Figure 9 compares the hygroscopicity

419 distributions of sea salt particles during P1&P3 and during P2&P4. As expected, the

420 hygroscopicity distribution during P1&P3 shifted slightly (ΔGF=-0.02) to lower GF, suggesting

421 more aged sea salt particles had reduced hygroscopicity, consistent with the trend discussed

422 previously. These results also demonstrate that the hygroscopicity estimation method is

423 sufficiently sensitive to reflect the minor changes in particle mass spectra to the estimated

424 hygroscopicity.

3.2.4 Particle type distributions in various hygroscopicity modes

426 The particles analyzed by ATOFMS during the studied period were classified within the same

427 classification scheme as HTDMA-ATOFMS experiment. With the estimated hygroscopicity of

428 individual particles, Figure 10 shows the number contributions of each particle type as a

429 function of GF. In the GF 0.9-1.1 range, the fresh EC and HMOC particles were dominant with

430 biomass and cooking types. In the GF 1.1-1.3 range, the Ammonium/OC particles is the most

431 abundant type, which contributed to nearly 40% particle numbers in this GF range. The main

432 particle type in the higher GF range (1.3-1.55) was aged EC particles. Sea salt particles were

433 present mainly in the narrower range of GF 1.55-1.65. A previous HTDMA characterization

434 study (Swietlicki et al., 2008) has suggested that ambient submicron particles have four

435 hygroscopicity modes, namely near-hydrophobic (NH), less-hygroscopic (LH), more-

436 hygroscopic (MH) and sea salt modes, with their GFs centered in 1.0-1.1, 1.11-1.33, >1.33

437 and >1.85 ranges, respectively (at 90% RH). These hygroscopicity modes correspond well to

438 the particle types analyzed in this study. Freshly emitted EC particles from combustion sources

439 and organic particles with higher molecular weight were the major contributors of nearly

440 hydrophobic (NH) mode in this study. Consistent with their particle mass spectra (Figure 2,

441 Figure S2), more-hygroscopic particles were hydrophilic due to condensation of nitrate and

442 sulfate. For the chemical composition of less-hygroscopic particles was rarely reported.

443 However, the present study indeed identified a unique particle type that is specifically enriched

444 in less-hygroscopic range. Both the HTDMA-ATOFMS experiment and ambient ATOFMS

445 sampling have suggested that their mass spectra contained many organic, ammonium and

446   sulfate signals. Temporal concentrations of this particle type indicate they were only enriched

447   in specific days in P1 and P3 period, as suggested in Figure 5. Their real sources and production

448   mechanisms deserve further investigations.

449   *4. CONCLUSIONS*

450   The hygroscopicity and composition of submicron particles were simultaneously characterized

451   in urban atmosphere (Shanghai). A single particle mass spectrometer, ATOFMS, was connected

452   to the downstream of HTDMA to analyze composition of hygroscopicity segregated particles.

453   A dataset linking single particle compositions and particle hygroscopicity was obtained.

454   Generally, biomass particles, fresh EC particles, organic particles with high molecular weight

455   (HMOC) were mostly present in NH particle mode. Hydrophilic particle types, including aged

456   EC, amine rich particles, usually have a GF>1.3. Cooking particles were exclusively detected

457   in GF< 1.1 range. Sea salt particles were present in very hygroscopic range (GF>1.5).

458   Atmospheric processing was shown to reduce the hygroscopicity of sea salt particles. A unique

459   Ammonium/OC particle type was identified to have a GF mode centered at 1.2, which is

460   assumed to originate from coal combustion.

461   In this study, based on the obtained hygroscopicity-composition relations, we developed a new

462   statistical method to estimate particle hygroscopicity just from its single particle mass spectra.

463   Individual particles were differentiated by the estimated hygroscopicity into various modes.

464   Consistent with the HTDMA hygroscopicity measurements, our estimated hygroscopicity

465   distribution shows three modes, namely near hydrophobic (NH) mode, more hygroscopic mode

466   (MH) and sea salt mode. The temporal profiles of estimated hygroscopicity distributions can

467   explain the variations of visibilities. This method is a novel way of single particle mass

468   spectrometry data analysis, which would provide critical new information on particulate water

469   content, particle source apportionment and aging process.

470   ***REFERENCES***

471   Andreae, M. O., and Rosenfeld, D.: Aerosol-cloud-precipitation interactions. Part 1. The nature and
472   sources of cloud-active aerosols, Earth-Sci. Rev., 89, 13-41, 10.1016/j.earscirev.2008.03.001, 2008.

473   Angelino, S., Suess, D. T., and Prather, K. A.: Formation of aerosol particles from reactions of
474   secondary and tertiary alkylamines: Characterization by aerosol time-of-flight mass spectrometry,
475   Environmental Science & Technology, 35, 3130-3138, 10.1021/es0015444, 2001.

476   Buzorius, G., Zelenyuk, A., Brechtel, F., and Imre, D.: Simultaneous determination of individual
477   ambient particle size, hygroscopicity and composition, Geophysical Research Letters, 29, 1974
478   10.1029/2001gl014221, 2002.

479   Chen, J., Zhao, C. S., Ma, N., Liu, P. F., Gobel, T., Hallbauer, E., Deng, Z. Z., Ran, L., Xu, W. Y.,
480   Liang, Z., Liu, H. J., Yan, P., Zhou, X. J., and Wiedensohler, A.: A parameterization of low visibilities
481   for hazy days in the North China Plain, Atmospheric Chemistry and Physics, 12, 4935-4950,
482   10.5194/acp-12-4935-2012, 2012.

483   Chen, Y., Tian, M., Huang, R.-J., Shi, G., Wang, H., Peng, C., Cao, J., Wang, Q., Zhang, S., Guo,
484   D., Zhang, L., and Yang, F.: Characterization of urban amine-containing particles in southwestern
485   China: seasonal variation, source, and processing, Atmospheric Chemistry and Physics, 19, 3245-
486   3255, 10.5194/acp-19-3245-2019, 2019.

487   Cheng, Y. F., Wiedensohler, A., Eichler, H., Heintzenberg, J., Tesche, M., Ansmann, A., Wendisch,
488   M., Su, H., Althausen, D., Herrmann, H., Gnauk, T., Bruggemann, E., Hu, M., and Zhang, Y. H.:
489   Relative humidity dependence of aerosol optical properties and direct radiative forcing in the surface
490   boundary layer at Xinken in Pearl River Delta of China: An observation based numerical study,
491   Atmospheric Environment, 42, 6373-6397, 10.1016/j.atmosenv.2008.04.009, 2008.

492   Crippa, M., DeCarlo, P. F., Slowik, J. G., Mohr, C., Heringa, M. F., Chirico, R., Poulain, L., Freutel,
493   F., Sciare, J., Cozic, J., Di Marco, C. F., Elsasser, M., Nicolas, J. B., Marchand, N., Abidi, E.,
494   Wiedensohler, A., Drewnick, F., Schneider, J., Borrmann, S., Nemitz, E., Zimmermann, R., Jaffrezo,
495   J. L., Prevot, A. S. H., and Baltensperger, U.: Wintertime aerosol chemical composition and source
496   apportionment of the organic fraction in the metropolitan area of Paris, Atmospheric Chemistry and
497   Physics, 13, 961-981, 10.5194/acp-13-961-2013, 2013.

498   Dall'Osto, M., Booth, M. J., Smith, W., Fisher, R., and Harrison, R. M.: A study of the size
499   distributions and the chemical characterization of airborne particles in the vicinity of a large
500   integrated steelworks, Aerosol Science and Technology, 42, 981-991, 10.1080/02786820802339587,
501   2008.

502   Dall'Osto, M., and Harrison, R. M.: Urban organic aerosols measured by single particle mass
503   spectrometry in the megacity of London, Atmospheric Chemistry and Physics, 12, 4127-4142,
504   10.5194/acp-12-4127-2012, 2012.

505   Dall'Osto, M., Ovadnevaite, J., Ceburnis, D., Martin, D., Healy, R. M., O'Connor, I. P., Kourtchev,

506   I., Sodeau, J. R., Wenger, J. C., and O'Dowd, C.: Characterization of urban aerosol in Cork city
507   (Ireland) using aerosol mass spectrometry, Atmos. Chem. Phys., 13, 4997-5015, 10.5194/acp-13-
508   4997-2013, 2013.

509   Denkenberger, K. A., Moffet, R. C., Holecek, J. C., Rebotier, T. P., and Prather, K. A.: Real-time,
510   single-particle measurements of oligomers in aged ambient aerosol particles, Environmental
511   Science & Technology, 41, 5439-5446, 10.1021/es070329l, 2007.

512   Facchini, M. C., Mircea, M., Fuzzi, S., and Charlson, R. J.: Cloud albedo enhancement by surface-
513   active organic solutes in growing droplets, Nature, 401, 257-259, 10.1038/45758, 1999.

514   Facchini, M. C., Rinaldi, M., Decesari, S., Carbone, C., Finessi, E., Mircea, M., Fuzzi, S., Ceburnis,
515   D., Flanagan, R., and Nilsson, E. D.: Primary submicron marine aerosol dominated by insoluble
516   organic colloids and aggregates, Geophysical Research Letters, 35, 2008.

517   Gard, E., Mayer, J. E., Morrical, B. D., Dienes, T., Fergenson, D. P., and Prather, K. A.: Real-time
518   analysis of individual atmospheric aerosol particles: Design and performance of a portable
519   ATOFMS, Analytical Chemistry, 69, 4083-4091, 10.1021/ac970540n, 1997.

520   Gard, E. E., Kleeman, M. J., Gross, D. S., Hughes, L. S., Allen, J. O., Morrical, B. D., Fergenson,
521   D. P., Dienes, T., Galli, M. E., Johnson, R. J., Cass, G. R., and Prather, K. A.: Direct observation of
522   heterogeneous   chemistry   in   the   atmosphere,   Science,   279,   1184-1187,
523   10.1126/science.279.5354.1184, 1998.

524   Gysel, M., Crosier, J., Topping, D. O., Whitehead, J. D., Bower, K. N., Cubison, M. J., Williams, P.
525   I., Flynn, M. J., McFiggans, G. B., and Coe, H.: Closure study between chemical composition and
526   hygroscopic growth of aerosol particles during TORCH2, Atmospheric Chemistry and Physics, 7,
527   6131-6144, 2007.

528   Healy, R. M., Hellebust, S., Kourtchev, I., Allanic, A., O'Connor, I. P., Bell, J. M., Healy, D. A.,
529   Sodeau, J. R., and Wenger, J. C.: Source apportionment of PM2.5 in Cork Harbour, Ireland using a
530   combination of single particle mass spectrometry and quantitative semi-continuous measurements,
531   Atmospheric Chemistry and Physics, 10, 9593-9613, 10.5194/acp-10-9593-2010, 2010.

532   Healy, R. M., Evans, G. J., Murphy, M., Juranyi, Z., Tritscher, T., Laborde, M., Weingartner, E.,
533   Gysel, M., Poulain, L., Kamilli, K. A., Wiedensohler, A., O'Connor, I. P., McGillicuddy, E., Sodeau,
534   J. R., and Wenger, J. C.: Predicting hygroscopic growth using single particle chemical composition
535   estimates, Journal of Geophysical Research-Atmospheres, 119, 9567-9577, 10.1002/2014jd021888,
536   2014.

537   Herich, H., Kammermann, L., Gysel, M., Weingartner, E., Baltensperger, U., Lohmann, U., and
538   Cziczo, D. J.: In situ determination of atmospheric aerosol composition as a function of hygroscopic
539   growth, Journal of Geophysical Research-Atmospheres, 113, D16213
540   10.1029/2008jd009954, 2008.

541   Herich, H., Kammermann, L., Friedman, B., Gross, D. S., Weingartner, E., Lohmann, U.,
542   Spichtinger, P., Gysel, M., Baltensperger, U., and Cziczo, D. J.: Subarctic atmospheric aerosol

543   composition: 2. Hygroscopic growth properties, Journal of Geophysical Research-Atmospheres,
544   114, D13204
545   10.1029/2008jd011574, 2009.

546   Herich, H., Hueglin, C., and Buchmann, B.: A 2.5 year's source apportionment study of black carbon
547   from wood burning and fossil fuel combustion at urban and rural sites in Switzerland, Atmospheric
548   Measurement Techniques, 4, 1409-1420, 10.5194/amt-4-1409-2011, 2011.

549   Kamilli, K. A., Poulain, L., Held, A., Nowak, A., Birmili, W., and Wiedensohler, A.: Hygroscopic
550   properties of the Paris urban aerosol in relation to its chemical composition, Atmospheric Chemistry
551   and Physics, 14, 737-749, 10.5194/acp-14-737-2014, 2014.

552   Koehler, K. A., Kreidenweis, S. M., DeMott, P. J., Petters, M. D., Prenni, A. J., and Carrico, C. M.:
553   Hygroscopicity and cloud droplet activation of mineral dust aerosol, Geophysical Research Letters,
554   36, L08805
555   10.1029/2009gl037348, 2009.

556   Laborde, M., Crippa, M., Tritscher, T., Juranyi, Z., Decarlo, P. F., Temime-Roussel, B., Marchand,
557   N., Eckhardt, S., Stohl, A., Baltensperger, U., Prevot, A. S. H., Weingartner, E., and Gysel, M.: Black
558   carbon physical properties and mixing state in the European megacity Paris, Atmospheric Chemistry
559   and Physics, 13, 5831-5856, 10.5194/acp-13-5831-2013, 2013.

560   Li, H., Wang, Q. g., Yang, M., Li, F., Wang, J., Sun, Y., Wang, C., Wu, H., and Qian, X.: Chemical
561   characterization and source apportionment of PM2.5 aerosols in a megacity of Southeast China,
562   Atmospheric Research, 181, 288-299, 10.1016/j.atmosres.2016.07.005, 2016.

563   Li, K., Ye, X., Pang, H., Lu, X., Chen, H., Wang, X., Yang, X., Chen, J., and Chen, Y.: Temporal
564   variations in the hygroscopicity and mixing state of black carbon aerosols in a polluted megacity
565   area, Atmospheric Chemistry and Physics, 18, 15201-15218, 10.5194/acp-18-15201-2018, 2018.

566   Liu, H. J., Zhao, C. S., Nekat, B., Ma, N., Wiedensohler, A., van Pinxteren, D., Spindler, G., Muller,
567   K., and Herrmann, H.: Aerosol hygroscopicity derived from size-segregated chemical composition
568   and its parameterization in the North China Plain, Atmospheric Chemistry and Physics, 14, 2525-
569   2539, 10.5194/acp-14-2525-2014, 2014.

570   Liu, P. F., Zhao, C. S., Gobel, T., Hallbauer, E., Nowak, A., Ran, L., Xu, W. Y., Deng, Z. Z., Ma, N.,
571   Mildenberger, K., Henning, S., Stratmann, F., and Wiedensohler, A.: Hygroscopic properties of
572   aerosol particles at high relative humidity and their diurnal variations in the North China Plain,
573   Atmospheric Chemistry and Physics, 11, 3479-3494, 10.5194/acp-11-3479-2011, 2011.

574   Liu, X. G., Zhang, Y. H., Cheng, Y. F., Hu, M., and Han, T. T.: Aerosol hygroscopicity and its impact
575   on atmospheric visibility and radiative forcing in Guangzhou during the 2006 PRIDE-PRD
576   campaign, Atmospheric Environment, 60, 59-67, 10.1016/j.atmosenv.2012.06.016, 2012.

577   Lohmann, U., and Feichter, J.: Global indirect aerosol effects: a review, Atmospheric Chemistry and
578   Physics, 5, 715-737, 2005.

579 Lohmann, U., Stier, P., Hoose, C., Ferrachat, S., Kloster, S., Roeckner, E., and Zhang, J.: Cloud
580 microphysics and aerosol indirect effects in the global climate model ECHAM5-HAM, Atmospheric
581 Chemistry and Physics, 7, 3425-3446, 2007.

582 Martin, M., Tritscher, T., Juranyi, Z., Heringa, M. F., Sierau, B., Weingartner, E., Chirico, R., Gysel,
583 M., Prevot, A. S. H., Baltensperger, U., and Lohmann, U.: Hygroscopic properties of fresh and aged
584 wood burning particles, Journal of Aerosol Science, 56, 15-29, 10.1016/j.jaerosci.2012.08.006,
585 2013.

586 Massling, A., Leinert, S., Wiedensohler, A., and Covert, D.: Hygroscopic growth of sub-micrometer
587 and one-micrometer aerosol particles measured during ACE-Asia, Atmos. Chem. Phys., 7, 3249-
588 3259, 10.5194/acp-7-3249-2007, 2007.

589 Pratt, K. A., Hatch, L. E., and Prather, K. A.: Seasonal Volatility Dependence of Ambient Particle
590 Phase Amines, Environmental Science & Technology, 43, 5276-5281, 10.1021/es803189n, 2009.

591 Qiu, C., and Zhang, R. Y.: Multiphase chemistry of atmospheric amines, Physical Chemistry
592 Chemical Physics, 15, 5738-5752, 10.1039/c3cp43446j, 2013.

593 Qu, W. J., Wang, J., Zhang, X. Y., Wang, D., and Sheng, L. F.: Influence of relative humidity on
594 aerosol composition: Impacts on light extinction and visibility impairment at two sites in coastal
595 area of China, Atmospheric Research, 153, 500-511, 10.1016/j.atmosres.2014.10.009, 2015.

596 Randles, C. A., Russell, L. M., and Ramaswamy, V.: Hygroscopic and optical properties of organic
597 sea salt aerosol and consequences for climate forcing, Geophysical Research Letters, 31,
598 10.1029/2004gl020628, 2004.

599 Rissler, J., Vestin, A., Swietlicki, E., Fisch, G., Zhou, J., Artaxo, P., and Andreae, M. O.: Size
600 distribution and hygroscopic properties of aerosol particles from dry-season biomass burning in
601 Amazonia, Atmospheric Chemistry and Physics, 6, 471-491, 2006.

602 Robinson, A. L., Subramanian, R., Donahue, N. M., Bernardo-Bricker, A., and Rogge, W. F.: Source
603 apportionment of molecular markers and organic aerosol. 3. Food cooking emissions,
604 Environmental Science & Technology, 40, 7820-7827, 10.1021/es060781p, 2006.

605 Shi, Y., Ge, M., and Wang, W.: Hygroscopicity of internally mixed aerosol particles containing
606 benzoic   acid   and   inorganic   salts,   Atmospheric   Environment,   60,   9-17,
607 http://dx.doi.org/10.1016/j.atmosenv.2012.06.034, 2012.

608 Silva, P. J., Liu, D. Y., Noble, C. A., and Prather, K. A.: Size and chemical characterization of
609 individual particles resulting from biomass burning of local Southern California species,
610 Environmental Science & Technology, 33, 3068-3076, 10.1021/es980544p, 1999.

611 Silva, P. J.: Source profiling and apportionment of airborne particles: A new approach using aerosol
612 time-of-flight mass spectrometry, Ph.D., University of California, Riverside, United States --
613 California, 428-428 p. pp., 2000.

614   Sjogren, S., Gysel, M., Weingartner, E., Alfarra, M. R., Duplissy, J., Cozic, J., Crosier, J., Coe, H.,
615   and Baltensperger, U.: Hygroscopicity of the submicrometer aerosol at the high-alpine site
616   Jungfraujoch, 3580 m a.s.l., Switzerland, Atmospheric Chemistry and Physics, 8, 5715-5729, 2008.

617   Song, X. H., Hopke, P. K., Fergenson, D. P., and Prather, K. A.: Classification of single particles
618   analyzed by ATOFMS using an artificial neural network, ART-2A, Analytical Chemistry, 71, 860-
619   865, 10.1021/ac9809682, 1999.

620   Su, Y. X., Sipin, M. F., Furutani, H., and Prather, K. A.: Development and characterization of an
621   aerosol time-of-flight mass spectrometer with increased detection efficiency, Analytical Chemistry,
622   76, 712-719, 10.1021/ac034797z, 2004.

623   Swietlicki, E., Hansson, H. C., Hameri, K., Svenningsson, B., Massling, A., McFiggans, G.,
624   McMurry, P. H., Petaja, T., Tunved, P., Gysel, M., Topping, D., Weingartner, E., Baltensperger, U.,
625   Rissler, J., Wiedensohler, A., and Kulmala, M.: Hygroscopic properties of submicrometer
626   atmospheric aerosol particles measured with H-TDMA instruments in various environments - a
627   review, Tellus Series B-Chemical and Physical Meteorology, 60, 432-469, 10.1111/j.1600-
628   0889.2008.00350.x, 2008.

629   Titos, G., Jefferson, A., Sheridan, P. J., Andrews, E., Lyamani, H., Alados-Arboledas, L., and Ogren,
630   J. A.: Aerosol light-scattering enhancement due to water uptake during the TCAP campaign,
631   Atmospheric Chemistry and Physics, 14, 7031-7043, 10.5194/acp-14-7031-2014, 2014.

632   Wang, X., Williams, B. J., Tang, Y., Huang, Y., Kong, L., Yang, X., and Biswas, P.: Characterization
633   of organic aerosol produced during pulverized coal combustion in a drop tube furnace, Atmos. Chem.
634   Phys., 13, 10919-10932, 10.5194/acp-13-10919-2013, 2013.

635   Wang, X., Shen, Y., Lin, Y., Pan, J., Zhang, Y., Louie, P. K. K., Li, M., and Fu, Q.: Atmospheric
636   pollution from ships and its impact on local air quality at a port site in Shanghai, Atmos. Chem.
637   Phys., 19, 6315-6330, 10.5194/acp-19-6315-2019, 2019.

638   Wang, X. F., Zhang, Y. P., Chen, H., Yang, X., Chen, J. M., and Geng, F. H.: Particulate Nitrate
639   Formation in a Highly Polluted Urban Area: A Case Study by Single-Particle Mass Spectrometry in
640   Shanghai, Environmental Science & Technology, 43, 3061-3066, 10.1021/es8020155, 2009.

641   Wang, X. N., Ye, X. N., Chen, H., Chen, J. M., Yang, X., and Gross, D. S.: Online hygroscopicity
642   and chemical measurement of urban aerosol in Shanghai, China, Atmospheric Environment, 95,
643   318-326, 10.1016/j.atmosenv.2014.06.051, 2014.

644   Weingartner, E., Burtscher, H., and Baltensperger, U.: Hygroscopic properties of carbon and diesel
645   soot particles, Atmospheric Environment, 31, 2311-2327, http://dx.doi.org/10.1016/S1352-
646   2310(97)00023-X, 1997.

647   Ye, X., Tang, C., Yin, Z., Chen, J., Ma, Z., Kong, L., Yang, X., Gao, W., and Geng, F.: Hygroscopic
648   growth of urban aerosol particles during the 2009 Mirage-Shanghai Campaign, Atmospheric
649   Environment, 64, 263-269, http://dx.doi.org/10.1016/j.atmosenv.2012.09.064, 2013.

650   Ye, X. N., Chen, T. Y., Hu, D. W., Yang, X., Chen, J. M., Zhang, R. Y., Khakuziv, A. F., and Wang,
651   L.: A Multifunctional HTDMA System with a Robust Temperature Control, Advances in
652   Atmospheric Sciences, 26, 1235-1240, 10.1007/s00376-009-8134-3, 2009.

653   Ye, X. N., Ma, Z., Hu, D. W., Yang, X., and Chen, J. M.: Size-resolved hygroscopicity of
654   submicrometer urban aerosols in Shanghai during wintertime, Atmospheric Research, 99, 353-364,
655   10.1016/j.atmosres.2010.11.008, 2011.

656   Zelenyuk, A., Imre, D., Han, J. H., and Oatis, S.: Simultaneous measurements of individual ambient
657   particle size, composition, effective density, and hygroscopicity, Analytical Chemistry, 80, 1401-
658   1407, 10.1021/ac701723v, 2008.

659   Zhang, Q., Jimenez, J. L., Canagaratna, M. R., Allan, J. D., Coe, H., Ulbrich, I., Alfarra, M. R.,
660   Takami, A., Middlebrook, A. M., Sun, Y. L., Dzepina, K., Dunlea, E., Docherty, K., DeCarlo, P. F.,
661   Salcedo, D., Onasch, T., Jayne, J. T., Miyoshi, T., Shimono, A., Hatakeyama, S., Takegawa, N.,
662   Kondo, Y., Schneider, J., Drewnick, F., Borrmann, S., Weimer, S., Demerjian, K., Williams, P.,
663   Bower, K., Bahreini, R., Cottrell, L., Griffin, R. J., Rautiainen, J., Sun, J. Y., Zhang, Y. M., and
664   Worsnop, D. R.: Ubiquity and dominance of oxygenated species in organic aerosols in
665   anthropogenically-influenced Northern Hemisphere midlatitudes, Geophysical Research Letters, 34,
666   L13801
667   10.1029/2007gl029979, 2007.

668   Zhang, Y. P., Wang, X. F., Chen, H., Yang, X., Chen, J. M., and Allen, J. O.: Source apportionment
669   of lead-containing aerosol particles in Shanghai using single particle mass spectrometry,
670   Chemosphere, 74, 501-507, 10.1016/j.chemosphere.2008.10.004, 2009.
671

672   Draxler, R. R. and Rolph, G. D.: HYSPLIT (Hybrid Single-Particle Lagrangian Integrated
673   Trajectory) model v 4.9, NOAA Air Resource Laboratory, Silver Spring MD, available at:
674   http://www. arl.noaa.gov/ready/hysplit4.html, 2019.
675
676

677   ***AUTHOR CONTRIBUTION***

678   Xinning Wang designed this study and conducted the experiments. Xiaofei Wang and Xin

679   Yang supervised this study and help with experiment design. Xinning Wang, Xiaofei Wang

680   and Xin Yang wrote the manuscript.

681   ***DATA AVAILABILITY***

682   All of the observation data and the codes used in this manuscript are available from the

683   corresponding author upon request (xiaofeiwang@fudan.edu.cn).

684   ***ACKNOWLEDGMENT***

685   This work was partially supported by the National Natural Science Foundation of China (Nos.

686   91544224, 21906024, 41775150, 41827804) and Shanghai Natural Science Foundation (No.

687   19ZR1404000).

688   ***COMPETING INTERESTS***

689   The authors declare that they have no conflict of interest.

690

691   ***FIGURES***
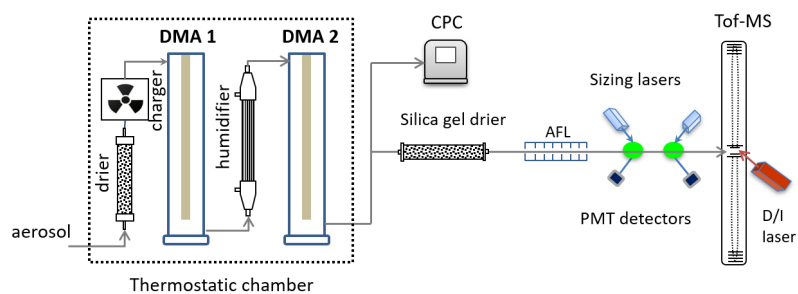
692

693   Figure 1. The schematic of HTDMA-ATOFMS characterization setup showing the major parts

694   of HTDMA (left), ATOFMS (right). The humidifier in HTDMA was maintained at 85% RH.

695
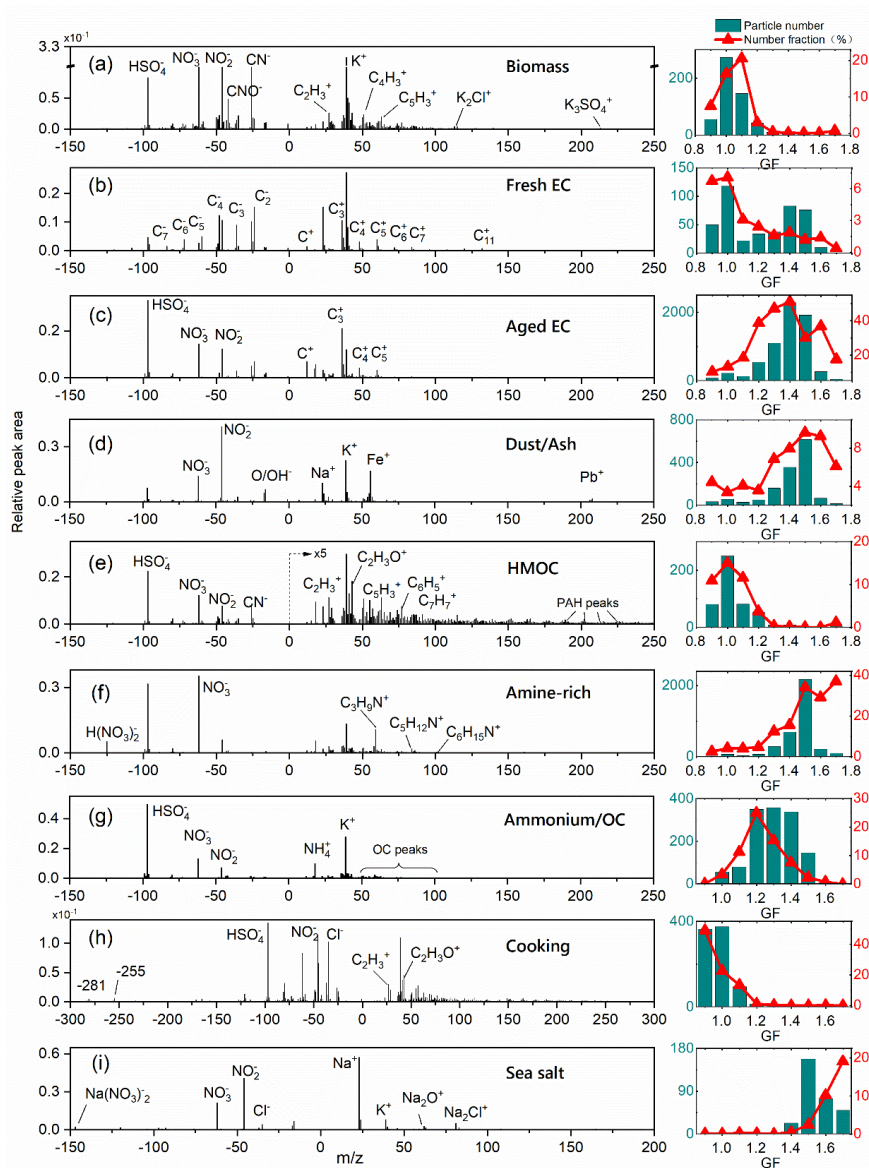
Figure 2. (Left panel) Averaged particle mass spectra of the major particle types detected in

HTDMA-ATOFMS characterization. Peaks of significance were labelled. Right panels show

the particle numbers of each type (left-axis) and their relative number fractions in total particles

699   (right-axis) as a function of GF.
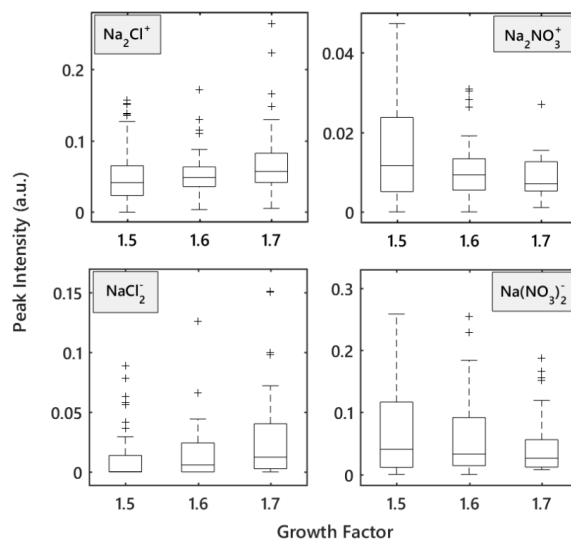
700

701   Figure 3. Statistics of relevant peak intensities in sea salt particle mass spectra detected at GF

702   1.5-1.7 range. The statistics are (from bottom to top): the minimum, 25th percentile, median,

703   75th percentile, maximum and outliers.

704
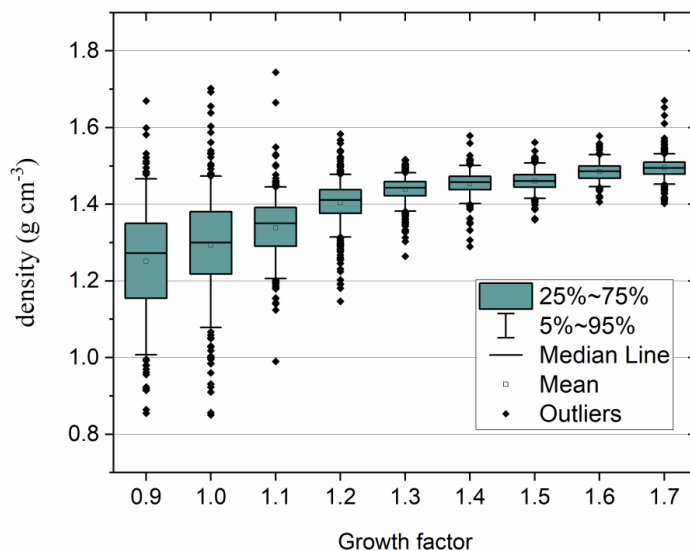
705

706 Figure 4. Particle effective densities of particles as a function of growth factor. The statistics

707 are (from bottom to top): the 5th percentile, 25th percentile, median, 75th percentile, 95th

708 percentile and outliers.

709

710
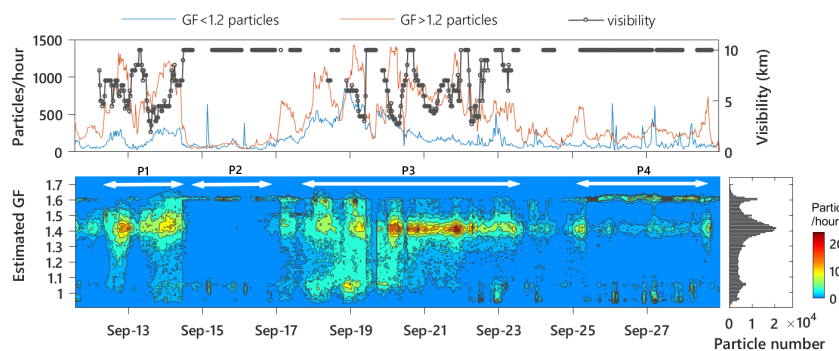
711

712   Figure 5. (Upper) Temporal variation of atmospheric visibility and particle concentrations of

713   Near Hydrophobic (estimated GF < 1.25) and More Hygroscopic (GF >1.25) mode. (Lower)

714   The contour plot illustrates the temporal variation of estimated GF from Sep-12 to Sep-28, 2012.

715   The lower-right panel denotes particle number distribution as a function of estimated GF during

716   the period.
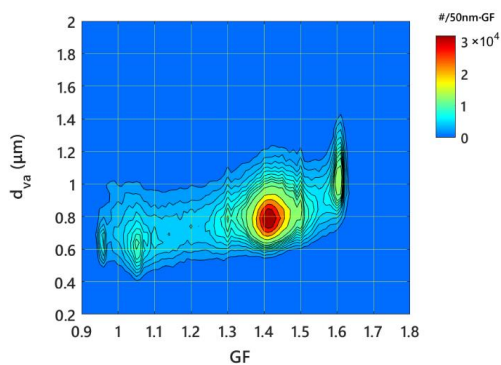
717

718   Figure 6. Contour plot of particle number concentrations as bivariate function of estimated GF

719   and aerodynamic diameter measured by ATOFMS.
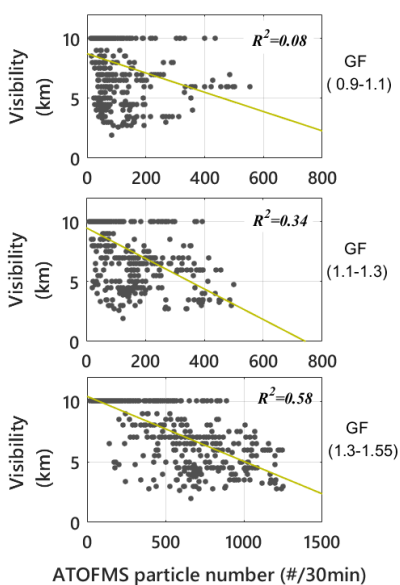
720

721   Figure 7. Correlation plots between visibility and ATOFMS particle numbers with the estimated

722   GF in 0.9-1.1, 1.1-1.3 and 1.3-1.55 range.

723

724
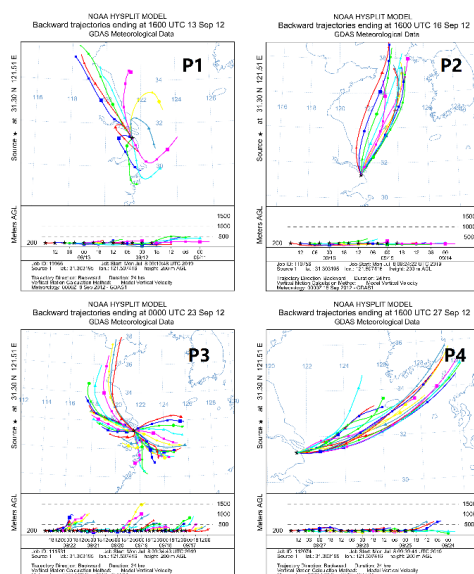
Figure 8. The 24-hour backward trajectories during P1 - P4 periods of the sampling site (by

HYSPLIT model).

727
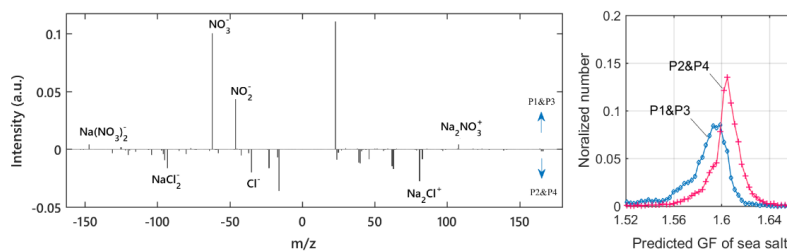
Figure 9. The differential mass spectrum between sea salt particles in (P1&P3) and (P2&P4).

Positive peaks indicate they are larger in P1&P3 than P2&P4. The right figure shows the

distributions of the predicted GF of sea salt in (P1&P3) and (P2&P4). Sea salt numbers were

normalized by their total numbers.

732

733
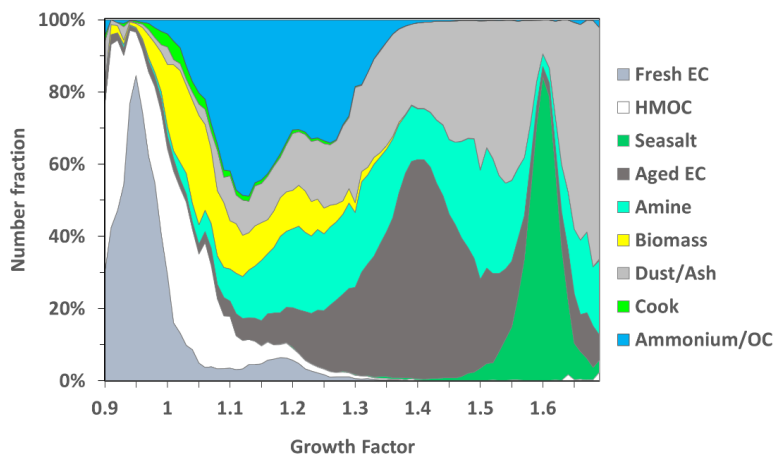
Figure 10. The number fractions of ATOFMS particle types as a function of estimated

hygroscopicity during Sep-12 to Sep-28, 2012.

736